Experimental measurement and expression of atmospheric ice Young's modulus according to its density

V. Palanque, E. Villeneuve, M. Budinger, V. Pommier-Budinger, G. Momen

Experimental measurement and expression of atmospheric ice Young's modulus according to its density

V. Palanque [a,b,*], E. Villeneuve [c,**], M. Budinger [d], V. Pommier-Budinger [b], G. Momen [c]

[a] ISAE-SUPAERO, University of Toulouse, 10 Avenue Edouard Belin, Toulouse 31400, France
[b] ONERA/MFE, University of Toulouse, F-31055 Toulouse, France
[c] AMIL, University of Quebec at Chicoutimi, 555 boulevard de l'Universite, G7H 2B1, Chicoutimi, Quebec, Canada
[d] Institut Clement Ader (ICA), University of Toulouse, INSA, ISAE-SUPAERO, MINES 9 ALBI, UPS, CNRS, 610101, France

Keywords:
Atmospheric ice
Young's modulus
Density
Cold room
Wind tunnel
Experimental
Numerical model

A B S T R A C T

Ice properties are hard to define and vary significantly in literature. While some of this variation can be attributed to different testing methods, the authors believe that most of this variation comes from the nature of the ice accretion itself. To address the problematic of scattering in mechanical properties values, a new approach is proposed which consists of expressing the behavior of atmospheric ice according to its density. Thanks to a hybrid experimental/numerical approach, the accurate measurement of the Young's modulus of atmospheric ice can be done. Ice samples are generated in both cold room and wind tunnel and at many different test conditions. The results obtained in this study confirm the validity of this new approach and gives a concrete relationship between the Young's modulus and the ice density. Finally, the relevance of using porous material hypothesis to explain the relation and the results domain of validity are discussed.

1. Introduction

Whether on the ground, in the air or at sea, icing conditions are encountered in cold regions across the world leaving natural or man-made structures covered in ice. When surrounding temperature is below the freezing point, suspended droplets in clouds or precipitations droplets become super-cooled droplets. Upon impinging on surfaces the freezing process is triggered and ice is created (Gent et al., 2000). The adhered ice constitutes a major threat for any architecture meeting structural constraints. In the transport field, infrastructures such as roads, rails but also vehicles themselves (ships, airplanes, helicopters, drones) are endangered due to icing. Because of the additional mass of the ice, telecommunication towers, electrical pylons and high voltage wires, are threatened with collapsing under their weight in poor weather conditions (1998 ice storm in North America). Furthermore, the accreted ice deteriorates the operation of structures such as wind turbines, rotor-blades and airfoil by altering their aerodynamics properties (Pouryoussefi et al., 2016; Shin and Bond, 1992; Etemaddar et al., 2014; Cao and Chen, 2010; Samad et al., 2021; Villeneuve et al., 2021a).

In many regards, the knowledge of the ice mechanical properties is of utmost interest. For instance, knowing ice mechanical properties such as its stiffness, its strength or even its density is mandatory to assess physical mechanisms leading to its mechanical shedding and therefore the development of mechanical ice protection systems (Laforte et al., 1998; Villeneuve et al., 2015; Villeneuve et al., 2020a; Villeneuve et al., 2020b; Villeneuve et al., 2020c; Ramanathan et al., 2000; Lin and Venna, 2002; Budinger et al., 2018; Pommier-Budinger et al., 2018; Budinger et al., 2021; Palanque et al., 2021; Labeas et al., 2006; Endres et al., 2017; Villeneuve et al., 2021b). Over the past century, many studies were conducted to measure the mechanical properties of ice. Among the most investigated properties, one can find the density, the Young's modulus, the cohesion strength, the adhesion strength and the critical energy release rate. The Young's modulus value is of special interest, as it is a key parameter in linear elastic theory. Knowing the elastic modulus enables the computation of stress fields and potential elastic energy (linked to energy release rate computation). Dorsey (Dorsey et al., 1940) gave a complete review of ice properties measured prior to 1940 and the measurement methods used. The reference ice entity is the single crystal of ordinary Ice Ih arranged in a tetrahedral way with oxygen atoms and water molecules separated by 2.76°A.

* Corresponding author at: ISAE-SUPAERO, University of Toulouse, 10 Avenue Edouard Belin, Toulouse 31400, France.
** Corresponding author at: AMIL, University of Quebec at Chicoutimi, 555 boulevard de l'Universite, G7H 2B1, Chicoutimi, Quebec, Canada.
E-mail addresses: valerian.palanque@isae-supaero.fr (V. Palanque), eric.villeneuve@uqac.ca (E. Villeneuve), mbudinge@insa-toulouse.fr (M. Budinger), valerie.budinger@isae-supaero.fr (V. Pommier-Budinger), gelareh.momen@uqac.ca (G. Momen).

https://doi.org/10.1016/j.coldregions.2023.103890

According to such arrangement, the density of the crystal can be estimated to 917 kg/m^3, being the reference density for pure ice (Mellor, 1980). The Young's modulus of the pure ice was investigated many times focusing on the behavior of a mono-crystal sample using standard material characterization tests. The mono crystal of ice Ih is by nature anisotropic and its properties were investigated by many researchers as described in (Mellor, 1980; Hobbs, 2010; Fletcher, 1970). However, in 1947, Northwood (Northwood, 1947) showed that the poly-crystalline ice Young's modulus was independent of the grain orientation through sound wave speed measurements and could therefore be considered as globally isotropic. Because of its granular constitution and the inherent existence of imperfection within the ice grain boundaries, the ice does not always follow standard elastic behavior. According to Hobbs (Hobbs, 2010), the elastic behavior of a crystal is due to changes in intermolecular distances, nevertheless, the ice impurities favor inter-grain movement. Under relatively progressive loading and large strain, grains can slip, reaching new equilibrium positions and therefore suffer from non-elastic deformation. Hence, it is assumed that load applied for short period with reduced strain magnitude would give little opportunity to trigger non-elastic behavior. For instance, Gold (Gold, 1958) defined maximum values for load (0.1 MPa) and strain rate (5 kPa.s^{-1}) preventing from miss-measuring inter grain displacement as elastic strain. Contrary to static (or quasi-static) measurements showing values of high discrepancy (0.3 GPa to 11 GPa) (Hobbs, 2010), dynamic measurements have given way less scattered values (Gold and Sinha, 1980). According to (Schulson, 1999), the standard value to use for poly-crystalline ice at -5 °C are 9.0 GPa for Young's modulus and 0.33 for Poisson ratio. The increase in the accuracy of Young's modulus measurement thanks to dynamic methods enabled to assess the influence of the density (Nakaya et al., 1959) on the stiffness. According to Nakaya's study on Greenland ice samples, a slight density decrease would lead in a stiffness loss. Gammon et al. (Gammon et al., 1983) showed using Brillouin Spectroscopy that for altered pure ice samples, on a local level, the Young's modulus of the crystal remains intact, however decreases on the global level of the ice sample. This can be explained by the presence of air bubbles, trapped in the freezing process replacing solid material. The influence of the density of the sea ice on its mechanical properties was investigated in (Frankenstein and Garner, 1970; Georges et al., 2021; Zong, 2022) showing that the stiffness and the strength of the ice tend to decrease with the density. In the case of atmospheric icing, the density is influenced by the temperature, the droplets velocity and the wetting intensity (Laforte et al., 1983; Druez et al., 1986; Kermani et al., 2008). However, atmospheric ice is mostly described in the literature from its visual aspect, being divided in three types: Glaze ice (transparent and compact), Rime ice (whitish and porous) and finally Mixed ice (combination of glaze and rime) (Scavuzzo and Chu, 1987). Consequently, its properties are usually expressed for given ice type which is mainly defined by the accretion temperature. Knowing the influence of continuous parameters such as temperature, flow rate and others on the icing phenomenon, the description of atmospheric ice to three well distinct categories appears to be limited.

The authors believe that much of the discrepancy observed in the atmospheric ice properties is caused by the difference in the ice samples obtained in each study, which can be attributed to the lack of a proper parameter allowing to universally characterize the ice, ensuring similarity in the ice samples generated. The objective of this paper is to characterize atmospheric ice Young's modulus in order to reduce variability between the values found in the literature, facilitating inter-laboratory comparison, covering the range of possible ice types in a more continuous way. This paper proposes a new approach in which the relationship between the ice Young's modulus and its corresponding density is investigated, which could make density the ideal parameter for ice accumulation characterization. The paper is organized as follows. First a hybrid method using both experimental and numerical approach to derive the Young's modulus for atmospheric ice samples of different densities is introduced. The method and the scientific means used for this study are described. Then, results of the study including an expression of the Young's modulus according to the density are given. An evaluation of the Weber number of the test conditions is then presented. Finally, this relation is discussed by considering ice as a porous material.

2. Method and material

The method consists in using modal finite element analyses compared to experimental measurements to determine the Young's modulus of ice. By exciting different resonance modes of a plate covered with ice and comparing the measured resonance frequencies with those calculated theoretically from a finite element model, the Young's modulus of the ice can be estimated thanks to a dynamic model. Various parameters influence the frequency of a structure, such as its mass, its stiffness and its geometry (stiffness and mass location). In the case of a plate covered with ice, the frequency depends on the substrate properties and on the ice parameters such as the ice position over the plate, the ice size (thickness, width and length), the ice stiffness (Young's modulus) and the ice mass and density. To simplify the study, it is decided to study a plate, fully covered with ice (removing ice location parameter) of homogeneous thickness (reducing complex geometry definition parameters to a single thickness). Therefore, in this simplified case, if the non-iced structure remains unmodified, the resonance frequencies depend on three parameters that vary according to the icing conditions: the ice layer thickness, the ice Young's modulus and finally the ice density. Therefore, by measuring the ice thickness, weighting the ice sample and observing its eigen modes frequencies, the corresponding Young's modulus can be computed numerically. The study is performed for various ice samples on metal substrates under different atmospheric icing conditions to obtain ice of different density values and to compute the Young's modulus versus ice density.

2.1. Numerical method for Young's modulus estimation

In order to avoid large numbers of iterative finite element computations (varying the Young's modulus value for each sample until frequency match is obtained), the idea is to obtain an analytical function expressing the frequency of the sample according to the three physical ice parameters identified previously (1).

$$Fmod = f(eice, Eice, \rho ice) \tag{1}$$

where e_{ice} is the thickness of the ice layer, E_{ice} the ice Young's modulus and ρ_{ice} the ice density.

This equation can be obtained by performing a linear regression on a previously computed well defined data set of finite element results. The boundaries of the data set are defined by the theoretical extreme values of the ice properties. According to literature, the density of the pure ice is set to 917 kg/m^3 (Mellor, 1980) and the corresponding maximum Young's modulus estimated is 9 GPa (Schulson, 1999). In the case of this study, it is decided not to exceed 5 mm of thickness for the ice layer as the irregularities in the ice shape tend to increase with the thickness. The minimum value for the ice thickness is set to 1 mm to ensure a observable influence of the ice on the structure, and for computational means. The minimum values for density and Young's modulus are arbitrarily chosen low enough according to the authors first assumptions. Table 1 shows the range of each parameter for the computations:

To minimize computation time and maximize the linear regression efficiency, a Latine Hypercube Sampling (LHS) design of experiment

Table 1
Range of parameters for the finite element computations.

	Density (kg/m^3)	Young's modulus (Pa)	Ice thickness (mm)
Range	[200−1000]	[0.5E9–9.5E9]	[1.0–5.0]

(DoE) is used (McKay et al., 1979). The domain is covered by the 236 points of the LHS DoE and 14 additional combinations are manually added to cover extremes points of the cubic domain (vertexes and faces centers). For each point of the DoE (a random combination of the three ice parameters is chosen within the domain boundaries), the first two frequencies are computed with software modal analysis.

Using PyVPLM application (De Giorgi et al., 2021), a linear regression is performed on the normalized data set. The coefficients of the polynomial expression are found while minimizing the mean error between the data set and the verification set. Therefore, for each sample, two polynomial equations are found to express the first and the second mode resonant frequencies according to the ice parameters. Finally, the roots of the polynomial are found using a Newton solver after inputting the measured frequency, thickness and density values into the equation. The Young's modulus value is easily retrieved by choosing the only root included in the Young's modulus range (Table 1).

2.2. Test sample definition

To execute the method introduced in this paper, ice must be accreted to a rigid body to allow the loading of the structure. In order to enable accurate estimation of ice properties, ice sensitive substrates are designed. The thickness of the substrate and its material are chosen to fit with aerospace airfoil standards: an aluminum sample (1.5 mm-thick) and a titanium sample (1 mm-thick) are machined. The samples are equipped with two 1 mm-thick piezo-electric ceramics (PIC 181). Ceramics are placed in a symmetric way to ensure the double axis-symmetry of the whole sample (Fig. 1). It is possible to use each of them either as sensor or actuator. The dimensions of the plate are chosen to match with results from Gold et.al study (Gold and Sinha, 1980) in which the authors showed that, as the load rate increases, the scattering of the Young's modulus measurement decreases, reaching an horizontal asymptotic for load rates above 5.0e2 Hz. Hence, the size of the sample is reduced to increase the first mode frequency of the titanium sample just above 0.5 kHz, ensuring that the loading of the ice will occur at sufficient rate.

A total of three titanium samples and one aluminum sample are machined. The samples dimensions are obtained accurately using a measuring column and are summarized in Table 2.

The piezoelectric devices are actuated using a sin wave generator. An acquisition card PCI-6221 device is used to retrieve the sensor electrical response. In order to avoid undesired structural damping and reduce the power required to actuate the structure, the system is vibrated in free conditions. The samples are tested in free boundary conditions, being suspended only by thin nylon strings.

A 3D finite element model of each substrate sample is realized using the FEM software ANSYS. The substrate, ice and ceramics are modeled with independent bodies and bonded using contact elements. A cubic linear meshing is applied to the bodies. No boundary conditions are set to the model in order to compute the modal response in free boundary conditions of the system. A preliminary study is realized to assess the validity of the models. The resonant frequencies of the first modes are computed through modal analysis for each of the bare (without ice) samples and compared with the experimental measured frequencies. The resulting numerical model discrepancy is under 2% for each sample, confirming their accuracy.

2.3. Icing process

As mentioned in literature (Gent et al., 2000; Druez et al., 1986; Kermani et al., 2008), the type of the ice encountered is highly related to the ambient temperature and precipitation rate (precipitation) or liquid water content (clouds). According to the continuity of the parameters of influence, characterizing ice simply as rime or glaze appears to be way too discretized, leading to significantly large ranges of values for their possible characteristics. For these reasons, a new approach to define ice

Table 2
Measurements of the four samples dimensions.

	Sample 1	Sample 3	Sample 4	Sample *Al*
Material	Ti TA6V	Ti TA6V	Ti TA6V	*Al* 5754
Thickness (mm)	1.10 ± 0.01	1.11 ± 0.01	1.11 ± 0.01	1.51 ± 0.01
Width (mm)	49.48 ± 0.15	49.68 ± 0.01	49.80 ± 0.10	49.32 ± 0.20
Length(mm)	130.27 ± 0.03	130.39 ± 0.04	131.08 ± 0.01	128.90 ± 0.05

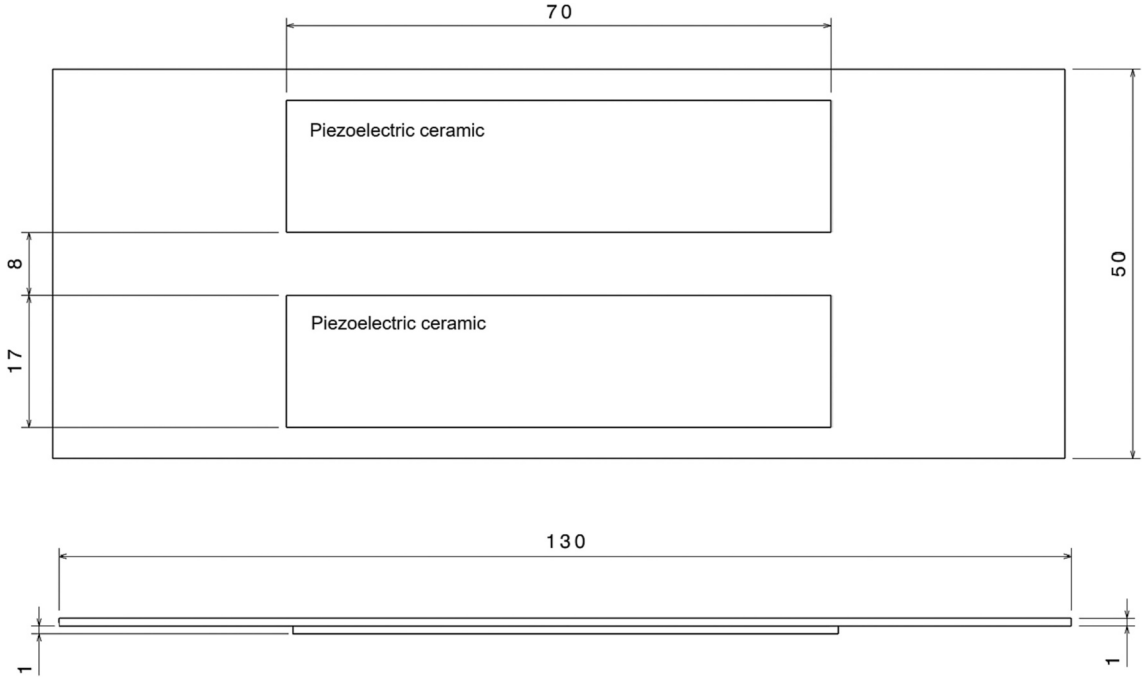

Fig. 1. Titanium substrate and ceramics configuration (in mm).

is explored, which consists in characterizing ice samples by their density. In order to validate this new approach, ice accumulations of different densities are obtained and their Young's modulus is measured as described previously. In addition, ice of similar densities are also obtained but for multiple different icing conditions, by varying both temperature and accumulation rate.

2.3.1. Cold room ice

The first ice samples generated for testing are obtained in a cold room. The cold room enables lowering the ambient temperature down to −40 °C and is equipped with an injection system allowing to create the icing conditions. The injection system is mounted on a rail fixed on the ceiling of the room. The water is injected at high pressure (70 bars) and pulverized into droplets of 320 μm median diameter using a spraying systems flat jet nozzle. Droplets then fall toward the accretion area through gravity. The injected water is demineralized and stored in a cooling tank at low temperature just above freezing point ([0–1]°C) before injection. The ice deposit realized in cold chamber is observed to be extremely uniform (mean deviation under 5%), which allows accurate measurements of the thickness to give a precise idea of the ice block volume.

Firstly, a design of experiment is developed to define the icing conditions according to two input parameters: precipitation rate and room temperature.

A central composite design of experiment is chosen, as it is recommended for experimental studies and reduces the amount of tests to be realized (Box and Wilson, 1992). A CCC (central composite circumscribed) design of experiment is selected. The boundaries of the CCC are defined by two constraints being the temperature, under −3 °C (to ensure freezing of the ice), and the liquid water saturation on the substrate. The liquid water saturation domain for this study is roughly assessed with preliminary injections and avoided to ensure the creation of representative impact ice. The temperature range of the DoE was maximized to extend the validity of the study between −5.8 °C and −24.2 °C. Linear regression is performed on the experimental data set and finally an expression of the density of the ice according to the room temperature and precipitation rate for this specific case is obtained (Fig. 2). The trend of the chart confirms that the same density should be obtainable for different temperatures, according to the flow rate used. According to the authors' experience, this map is only valid for the samples studied and would not be applicable for substrates with different thermal mass.

Secondly, the ice samples are realized and characterized. The same icing condition is repeated a few times to study the repeatability of the injection process. For each repetition, ice is accreted over the three titanium samples at the same time. After the accumulation, the ice thickness is measured in three positions along the length of the sample using a Vernier caliper. Then the mean thickness is assessed for the whole layer. The samples are weighted inside the cold room. The mean thickness, the mass and the density are therefore known for each sample. The results of the first six injections are shown Table 3. Four of these injections are realized over a total time of sixty minutes (Injection n°4 to n°7), whereas the last two injections are realized over a total time of ninety minutes (Injection n°8 and n°9), which led to mass and thickness differences, while the density remains constant, as the temperature and the precipitation rate are kept constant.

Figs. 3, 4 show two ice samples of same density obtained with two different temperatures, highlighting the influence of the flow rate over density and demonstrating that it is function of multiple different parameters.

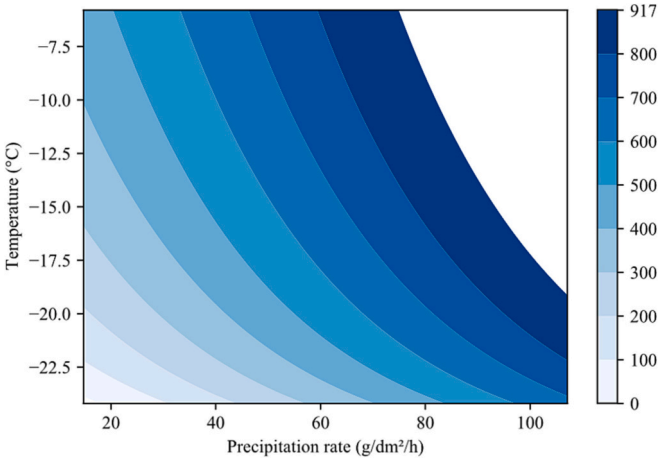

Fig. 2. Density (kg/m^3) model according to the freezing temperature (°C) and the precipitation rate (g/dm^2/h) for this specific case.

2.3.2. Wind tunnel ice

To further confirm that ice samples can be defined using their densities, the study is extended to impact ice generated in an icing wind tunnel. The wind tunnel is a closed-loop tunnel that can be refrigerated down to −40 °C and equipped with sprinkler ramps to generate icing precipitations. The smallest test section, which turns out to be compatible with the small size of the test plates, is used to obtain the maximum wind speed. The section is 500 mm × 600 mm and speeds up to 50 m/s can be obtained while maintaining temperatures down to −25 °C. The LWC of the wind tunnel is calibrated for values of 0.3 and 1.0 g/m^3 using a hot wire probe. The droplet Median Volumetric Diameter (MVD) is 25 μm. A new design of experiment is realized. The sample is maintained in the study zone thanks to a rigid aluminum interface. The sample is placed perpendicular to the wind direction in the center of vein to harmonize the surrounding air flow. The test section of the wind tunnel is surrounded by a cold chamber, enabling to extract the samples from the tunnel at freezing temperature to perform measurements on the ice. Four different injection conditions are selected by modifying the flow rate of the injectors resulting in intermediate LWC values in the [0.3–1.0] range. Two velocities are investigated. Table 4 summarizes the different injection parameters.

Contrary to cold room ice samples, the ice shapes obtained are more irregular due to the air flow surrounding the substrate. As a consequence, the modeling of the ice shape is less simple and each ice sample requires a dedicated 3D modeling. To maximize the accuracy of the model, measurements are taken at nine different positions. The density is estimated thanks to the 3D model volume. An example of the ice shape and its 3D ice model are given Fig. 5.

3. Results

3.1. Cold room results

The DoE described in 2.3.1 is extended by adding many other points considered of interest by the authors (extremes conditions out of the DoE range). A total of 44 ice samples are generated.

Table 3
Density of the ice samples for each injection.

	Sample 1	Sample 3	Sample 4
Injection 4	6,82E+02	6,75E+02	
Injection 5	6,32E+02	6,21E+02	6,78E+02
Injection 6	6,65E+02	6,85E+02	6,85E+02
Injection 7	6,65E+02	6,64E+02	6,92E+02
Injection 8	6,59E+02	6,84E+02	7,26E+02
Injection 9	6,59E+02	7,26E+02	7,11E+02
Mean deviation	2%	5%	3%
Max deviation	3.5%	7.5%	3.5%
Total mean deviation		4%	
Total max deviation		7.5%	

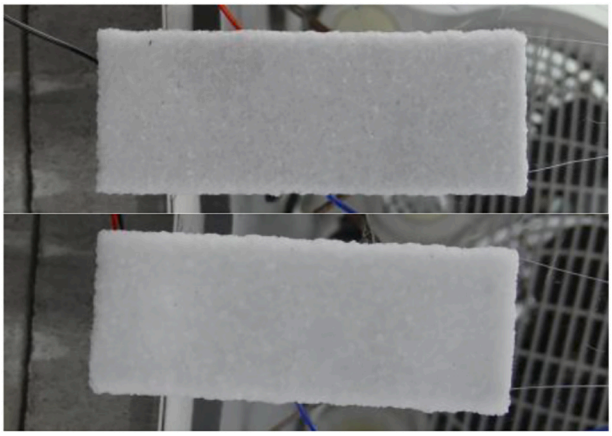

Fig. 3. Two ice samples showing.

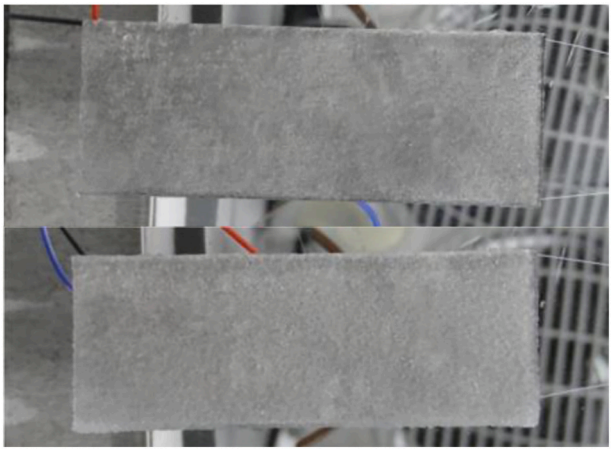

Fig. 4. Two ice samples showing similar density (453 and 465 kg/m^3) similar density (816 and 807 kg/m^3) obtained with two different room obtained with two different room temperatures (−15 °C and - 21.5 °C) temperatures (−5.8 °C and - 8.5 °C).

Table 4
Parameters used for wind tunnel ice sample generation.

Temperature (°C)	[−5, −8.5, −13, −15, −20, −25]
LWC (g/cm^3)	[0.3, 0.5, 0.8, 1.0]
Velocity (m/s)	[30, 50]
MVD (μm)	(Fletcher, 1970)

For each sample obtained, the frequencies of the first two resonant modes of flexion are measured using one piezo-ceramic as actuator. The magnitude of the input signal is set to 10 V to remain in small strain ranges to avoid deicing. A first large sweep is realized in a [10.5 kHz - 0.5 kHz] range to give a rough idea of the frequencies of the resonant modes in this interval. Then, a finer sweep is used to measure with precision the frequency of each mode.

The vibration magnitude is measured using the second piezo-ceramic as a sensor. The frequencies are retrieved in post treatment with a ± 5 Hz precision giving a maximum error inferior to 1%. An example of the frequency spectrum obtained for the large sweep is shown in Fig. 6.

Using the method described in 2.1, the density, the thickness and the frequency of the modes are entered into a solver and the Young's modulus is estimated. The numerical error of the model is assessed by checking the influence of small variations in the inputs on the overall solution. According to the propagation uncertainty theory, the uncertainty over the density measurement can be expressed thanks to Eq. (2). It is therefore possible to compute the uncertainty on the Young's modulus values according to the uncertainties on the measurements $\delta\rho$, δf and δe (Fig. 7).

$$\frac{\delta\rho}{\rho} = \frac{\delta e}{e} + \frac{\delta m}{m} \tag{2}$$

For each sample, the computed Young's modulus can be plotted in function of the measured density of the ice. For each injection, the young's modulus is estimated using the first mode frequency and the second mode frequency. The results obtained for each of both Sample 1 and Sample *Al* configurations are shown in Fig. 8. Results show that, whatever the sample and its material and whatever the mode, the trend of data set is highly similar. Therefore, all data are displayed on the same graph and the expression of the ice Young's modulus according to the density can be defined (Fig. 9).

From Fig. 9, the following polynomial, expressing the Young's modulus value according to its density, can be drawn (3)

$$E = E_0\left[1.416\left(\frac{\rho}{\rho_0}\right)^3 - 3.612\mathrm{e}^{-01}\left(\frac{\rho}{\rho_0}\right)^2 - 4.511\mathrm{e}^{-02}\left(\frac{\rho}{\rho_0}\right)\right] \tag{3}$$

with E_0 the Young's modulus with maximum density (9.0 GPa) and ρ_0 the density of pure ice (917 kg/m^3) (Mellor, 1980; Schulson, 1999).

Following this equation, an absolute uncertainty on the measurement of the density (measurement accuracy for instance) implies an uncertainty on the corresponding Young's modulus value. The analytical expression of this uncertainty ΔE can be expressed according to the density uncertainty $\Delta\rho$ and the density ρ (only for low $\Delta\rho/\rho$ ratio):

$$\Delta\mathrm{E} = \Delta\rho\left(3A_0\rho^2 + 2B_0\rho + C_0\right) \tag{4}$$

with $A_0 = 1.416\frac{E_0}{{\rho_0}^3}$, $B_0 = -3.612e^{-1}\frac{E_0}{{\rho_0}^2}$, and $C_0 = -4.511e^{-2}\frac{E_0}{\rho_0}$,

3.2. Wind tunnel results

Because of the irregularity of the ice shape, a finite element modal analysis is run for each geometry. The estimated density is given by the 3D model volume computation as explained previously and the Young's modulus is found by following a dichotomy process until the first mode

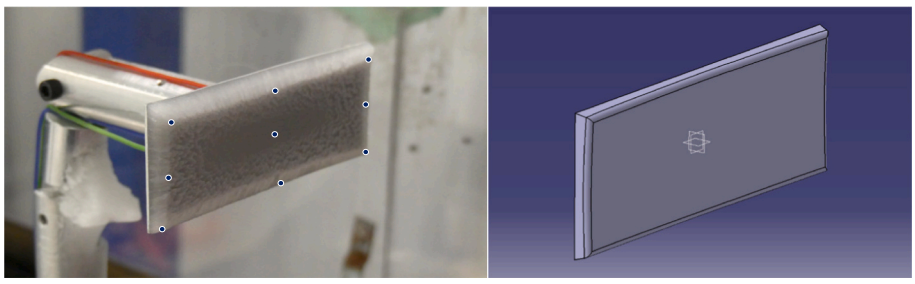

Fig. 5. Example of sample in the wind tunnel ice with the nine thickness measure locations and its 3D model.

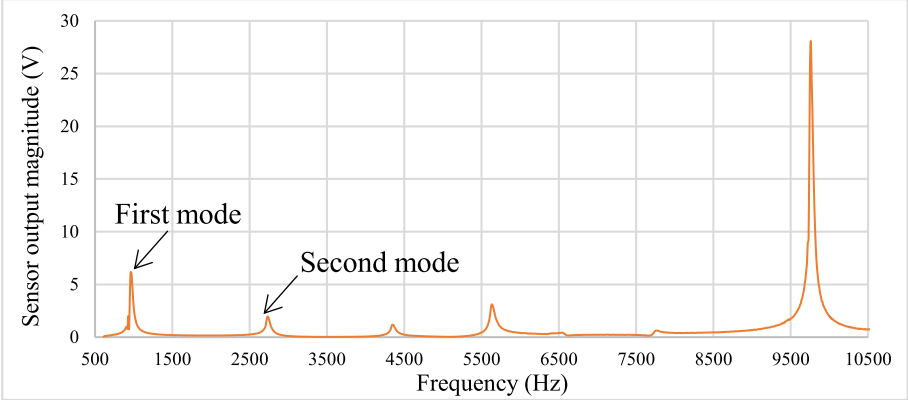

Fig. 6. Frequency spectrum for large sweep.

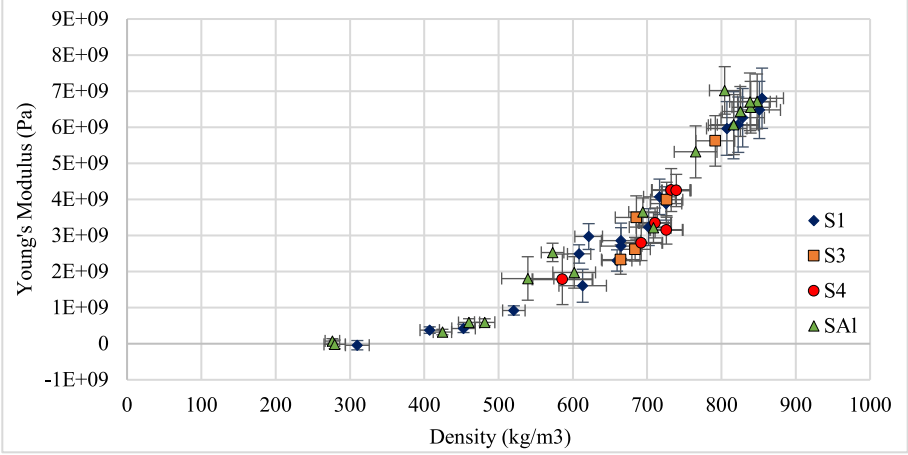

Fig. 7. Uncertainty over the Young's Modulus and the density according to numerical model.

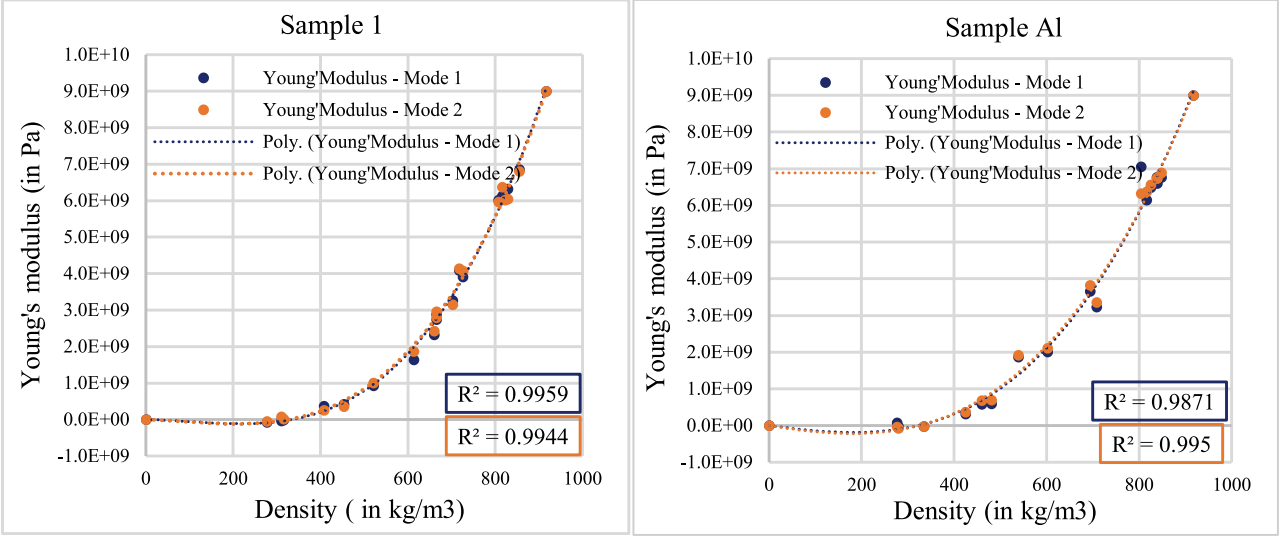

Fig. 8. Young's modulus according to the density for both modes and both Sample 1 and Sample *Al*.

frequency matches with the experimental one with under 1 Hz difference. Then, the Young's modulus according to the density can be plotted. The data obtained in the wind tunnel are considered as one set of data independent of the tunnel parameters (wind speed, LWC, Temperature) and, when displayed on the plot of the cold room data (Fig. 9), all the data seem to follow the same trend, and hence, the same law. It is important to mention that the droplets MVD also varied between the cold room and the icing wind tunnel. Relation (3) therefore allow describing the Young's modulus of any atmospheric ice according to its density only.

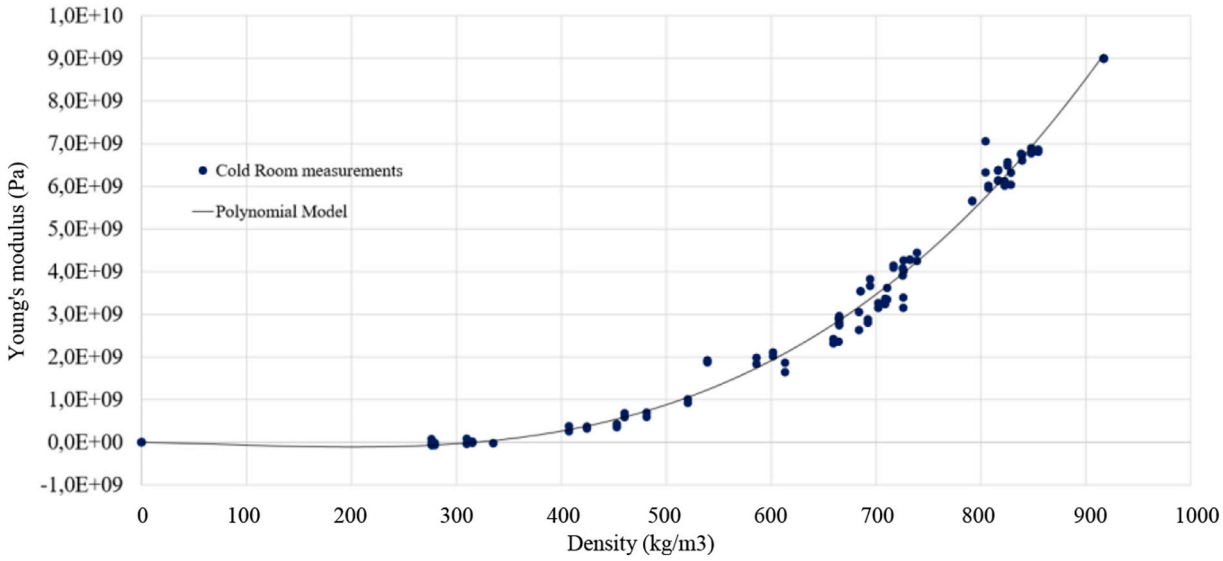

Fig. 9. Young's modulus according to the density for every cold room configuration.

4. Discussion

As shown in the result section, the density seems to be a dominant parameter in the definition of the ice stiffness. It appears from this study that density alone can be used to assess the Young's modulus of the ice. Ice could therefore be considered as a porous material as it was done for sea ice in (Zong, 2022). In literature, many models are described to assess the Young's modulus of a material according to its relative density i.e. porosity. According to (Kov'acik, 1999) which proposed a percolation model, the Young's modulus can be described as:

$$E = E_0\left(\frac{p_c - p}{p_c}\right)^f \tag{5}$$

with E the penalized Young's modulus, E_0 the pure Young's modulus of the material with full density ($p = 0$), p_c the porosity over which the Young's modulus is set to 0 and f the percolation theory exponent.

In this case, the pure material Young's modulus E_0, can be set to 9.0e9 Pa (Schulson, 1999) for a density of 917 kg/m^3 (Mellor, 1980). The p_c value is assessed using the experimental results obtained previously. Following the data set trend (Fig. 10), the critical porosity (porosity corresponding to a total loss of stiffness) seems to be reached at the density of 300 kg/m^3 corresponding to a porosity of 0.674. As explained in the paper (Schulson, 1999), the exponent value f is set to 2.1 in the case of 3D considerations. By applying these parameters to the equation, the following curve is defined (Fig. 11). The porosity model seems to match accurately with the previously obtained curves which comforts the authors in believing that the data set is relevant.

Using multiple icing conditions, the atmospheric ice Young's modulus appears to be, within the range of interest in this study, independent of the temperature, the air velocity and the droplet size in the first order. The stiffness behavior of a porous material is linked to the shape of the porous cavities (Schulson, 1999). The assumption is made that for a given droplet impact regime, the arrangement of the porous material remains constant. According to droplet impact works (Garcia et al., 2008; Castanet et al., 2009) the droplet impact regime on a flat wall can be described according to the K dimensionless number, being a product of Weber and Ohnesorge numbers (6).

$$K = WeOh^{-2/5} \tag{6}$$

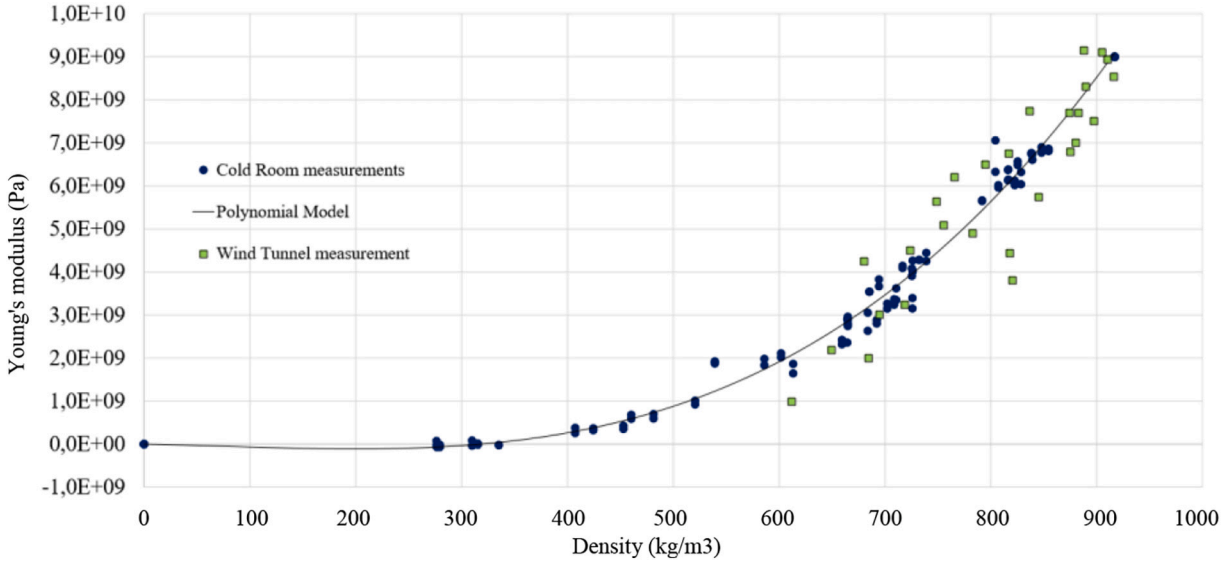

Fig. 10. Young's modulus according to the density for every cold room and wind tunnel configurations.

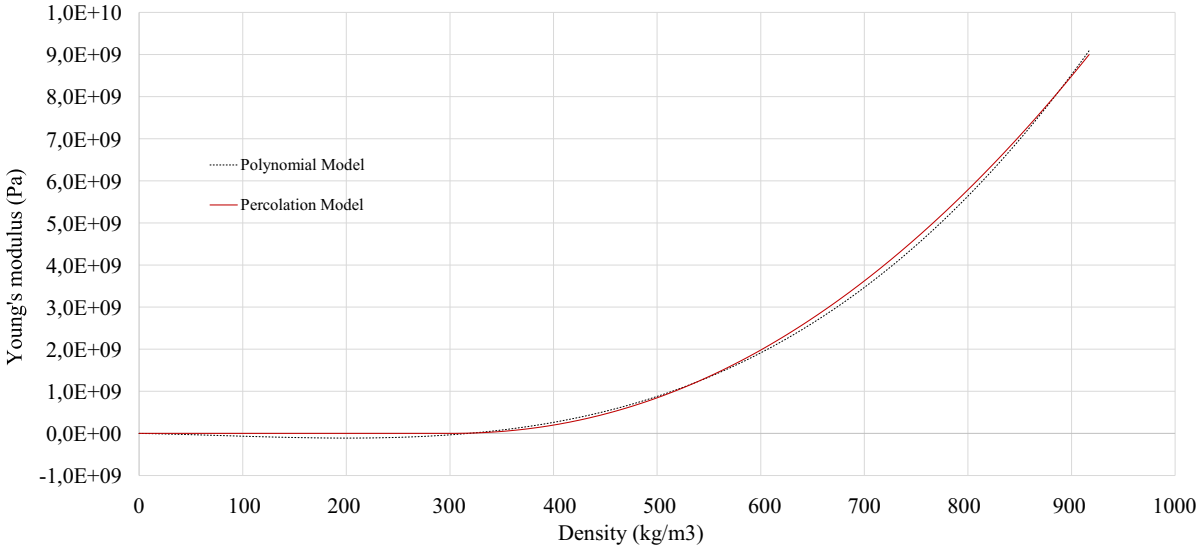

Fig. 11. Polynomial model versus percolation model.

For wall with subzero temperatures, the regime of impact is observed as"splashing" for K conditions above $K_c = 3500$ and"deposition" for K conditions under 3500 (Garcia et al., 2008). Using regular aviation data, a simplified map of the K parameter for standard in-flight icing conditions can be computed (Fig. 12). The K_c threshold position shows that the results obtained in this study are obtained in droplet impact regimes broadly encountered in-flight, encouraging the authors in thinking that the model obtained is suitable for aircraft icing definition. Moreover, to the authors knowledge, there is not any direct evidence that a shift in the impact regime would influence the relation between density and Young's modulus of the impact ice.

5. Conclusion

A hybrid experimental/numerical method has been developed in accordance with literature recommendations, to assess the atmospheric ice Young's modulus with accuracy. This method was used to estimate the Young's modulus of ice samples generated both in cold chamber and wind tunnel. The experiments showed the Young's modulus can be defined as a function of ice density alone, and that parameters such as temperature, droplet size, flow velocity, or even LWC are only influencing Young's modulus through the ice density. An expression of the Young's modulus based on the interpolation of experiments results is established according to the density and a porosity model of this Young's modulus based on percolation model is also given in this paper, demonstrating the validity of the approach. Further study will be done to validate the approach for other ice material parameters such as the Poisson's ratio and the tensile strength.

CRediT authorship contribution statement

V. Palanque: Conceptualization, Methodology, Data curation, Software, Validation, Investigation, Writing – original draft. **E. Villeneuve:** Conceptualization, Supervision, Methodology, Writing – review & editing. **M. Budinger:** Conceptualization, Methodology, Writing – review & editing, Supervision. **V. Pommier-Budinger:** Resources,

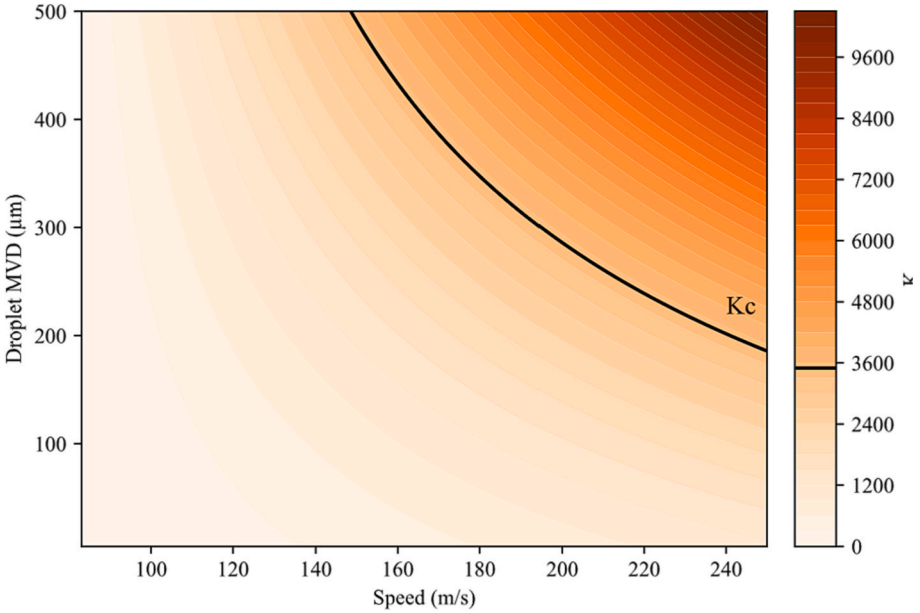

Fig. 12. K number according to flow speed (m/s) and the droplets MVD (µm) for $T = 0$ °C and P = P*atm.*

Writing – review & editing, Supervision. **G. Momen:** Funding acquisition, Project administration, Resources, Writing – review & editing.

Declaration of Competing Interest

The authors declare that they have no known competing financial interests or personal relationships that could have appeared to influence the work reported in this paper.

Data availability

Data will be made available on request.

References

Box, G.E., Wilson, K.B., 1992. On the Experimental Attainment of Optimum Conditions, 270–310.

Budinger, M., Pommier-Budinger, V., Bennani, L., Rouset, P., Bonaccurso, E., Dezitter, F., 2018. Electromechanical resonant ice protection systems: analysis of fracture propagation mechanisms. AIAA J. 56 (11), 4412–4422. https://doi.org/10.2514/1.J056663. Accessed 2020-05-06.

Budinger, M., Pommier-Budinger, V., Reysset, A., Palanque, V., 2021. Electromechanical resonant ice protection systems: energetic and power considerations. AIAA J. 59 (7), 2590–2602. https://doi.org/10.2514/1.J060008.

Cao, Y., Chen, K., 2010. Helicopter icing. The. Aeronaut. J. 114 (1152), 83–90.

Castanet, G., Li'enart, T., Lemoine, F., 2009. Dynamics and temperature of droplets impacting onto a heated wall. Int. J. Heat Mass Transf. 52 (3–4), 670–679.

De Giorgi, F., Budinger, M., Hazyuk, I., Reysset, A., Sanchez, F., 2021. Reusable surrogate models for the preliminary design of aircraft application systems. AIAA J. 59 (7), 2490–2502.

Dorsey, N.E., et al., 1940. Properties of Ordinary Water-Substance in all its Phases.

Druez, J., Nguyen, D.D., Lavoie, Y., 1986. Mechanical properties of atmospheric ice. Cold Reg. Sci. Technol. 13 (1), 67–74. https://doi.org/10.1016/0165-232X(86)90008-X.

Endres, M., Sommerwerk, H., Mendig, C., Sinapius, M., Horst, P., 2017. Experimental study of two electro-mechanical de-icing systems applied on a wing section tested in an icing wind tunnel. CEAS Aeronaut. J. 8 (3), 429–439.

Etemaddar, M., Hansen, M.O.L., Moan, T., 2014. Wind turbine aerodynamic response under atmospheric icing conditions. Wind Energy 17 (2), 241–265.

Fletcher, N.H., 1970. Mechanical properties. Cambridge Monographs on Physics. Cambridge University Press, pp. 165–197. https://doi.org/10.1017/CBO9780511735639.010.

Frankenstein, G.E., Garner, R., 1970. Dynamic Young's Modulus and Flexural Strength of Sea Ice, 222.

Gammon, P.H., Kiefte, H., Clouter, M.J., Denner, W.W., 1983. Elastic constants of artificial and natural ice samples by brillouin spectroscopy. J. Glaciol. 29 (103), 433–460. https://doi.org/10.3189/S0022143000030355.

Garcia, N., Villedieu, P., Dewitte, J., Lavergne, G., 2008. A New Droplet-Wall Interaction Model.

Gent, R.W., Dart, N.P., Cansdale, J.T., 2000. Aircraft icing. Philos. Trans. R. Soc. London, Ser. A 358 (1776), 2873–2911.

Georges, D., Saletti, D., Montagnat, M., Forquin, P., Hagenmuller, P., 2021. Influence of porosity on ice dynamic tensile behavior as assessed by spalling tests. J. Dyn. Behav. Mater. 7 (4), 575–590.

Gold, L.W., 1958. Some observations on the dependence of strain on stress for ice. Can. J. Phys. 36 (10), 1265–1275. https://doi.org/10.1139/p58-131.

Gold, L., Sinha, N., 1980. The Rheological Behaviour of Ice at Small Strains, 117–128.

Hobbs, P.V., 2010. Ice Physics. Google-Books-ID: 7Is6AwAAQBAJ.

Kermani, M., Farzaneh, M., Gagnon, R., 2008. Bending strength and effective modulus of atmospheric ice. Cold Reg. Sci. Technol. 53, 162–169. https://doi.org/10.1016/j.coldregions.2007.08.006.

Kov'acik, J., 1999. Correlation between young's modulus and porosity in porous materials. J. Mater. Sci. Lett. 18 (13), 1007–1010.

Labeas, G.N., Diamantakos, I.D., Sunaric, M.M., 2006. Simulation of the electroimpulse de-icing process of aircraft wings. J. Aircr. 43 (6), 1876–1885.

Laforte, J.-L., Phan, L.C., Felin, B., 1983. Microstructure of ice accretions grown on aluminum conductors. J. Appl. Meteorol. Climatol. 22 (7), 1175–1189. https://doi.org/10.1175/1520–0450(1983)022⟨1175:MOIAGO⟩2.0.CO;2.

Laforte, J.L., Allaire, M.A., Laflamme, J., 1998. State-of-the-art on power line de-icing. Atmos. Res. 46 (1), 143–158. https://doi.org/10.1016/S0169-8095(97)00057-4.

Lin, Y., Venna, S.V., 2002. Inflight deicing of self-actuating aircraft wing structures with piezoelectric actuators. In: ASME 2002 International Mechanical Engineering Congress and Exposition. American Society of Mechanical Engineers, pp. 243–247. In: https://proceedings. In: asmedigitalcollection.asme.org/proceeding.aspx?articleid=1580344.

McKay, M.D., Beckman, R.J., Conover, W.J., 1979. A comparison of three methods for selecting values of input variables in the analysis of output from a computer code. Technometrics 21 (2), 239–245.

Mellor, M., 1980. Mechanical Properties of Polycrystalline Ice, 217–245.

Nakaya, U., et al., 1959. Visco-Elastic Properties of Processed Snow.

Northwood, T., 1947. Sonic determination of the elastic properties of ice. Can. J. Res. 25 (2), 88–95.

Palanque, V., Budinger, M., Pommier-Budinger, V., Bennani, L., Delsart, D., 2021. Electro-mechanical resonant ice protection systems: Power requirements for fractures initiation and propagation. In: AIAA Aviation 2021 Forum. AIAA Aviation Forum. American Institute of Aeronautics and Astronautics. https://doi.org/10.2514/6.2021–2651. https://arc.aiaa.org/doi/10.2514/6.2021-2651. Accessed 2021-08-02.

Pommier-Budinger, V., Budinger, M., Rouset, P., Dezitter, F., Huet, F., Wetterwald, M., Bonaccurso, E., 2018. Electromechanical resonant ice protection systems: initiation of fractures with piezoelectric actuators. AIAA J. 56 (11), 4400–4411. https://doi.org/10.2514/1.J056662. Accessed 2020-05-06.

Pouryoussefi, S.G., Mirzaei, M., Nazemi, M.-M., Fouladi, M., Doostmahmoudi, A., 2016. Experimental study of ice accretion effects on aerodynamic performance of an naca 23012 airfoil. Chin. J. Aeronaut. 29 (3), 585–595. https://doi.org/10.1016/j.cja.2016.03.002.

Ramanathan, S., Varadan, V.V., Varadan, V.K., 2000. Deicing of helicopter blades using piezoelectric actuators. In: Smart Structures and Materials 2000: Smart Electronics and MEMS, vol. 3990, pp. 281–293. https://doi.org/10.1117/12.388906. International Society for Optics and Photonics. https://www. spiedigitallibrary.org/conference-proceedings-of-spie/3990/0000/ Deicing-of-helicopter-blades-using-piezoelectric-actuators/10.1117/12. 388906.short?SSO=1.

Samad, A., Villeneuve, E., Blackburn, C., Morency, F., Volat, C., 2021. An experimental investigation of the convective heat transfer on a small helicopter rotor with anti-icing and de-icing test setups. Aerospace 8. https://doi.org/10.3390/aerospace8040096.

Scavuzzo, R., Chu, M.L., 1987. Structural Properties of Impact Ices Accreted on Aircraft Structures. Technical Report.

Schulson, E.M., 1999. The structure and mechanical behavior of ice. Jom 51 (2), 21–27.

Shin, J., Bond, T., 1992. Results of an icing test on a naca 0012 airfoil in the nasa lewis icing research tunnel. In: 30th Aerospace Sciences Meeting and Exhibit, p. 647.

Villeneuve, E., Harvey, D., Zimcik, D., Aubert, R., Perron, J., 2015. Piezoelectric deicing system for rotorcraft. J. Am. Helicopter Soc. 60 (4), 1–12.

Villeneuve, E., Volat, C., Ghinet, S., 2020a. Numerical and experimental investigation of the design of a piezoelectric de-icing system for small rotorcraft part 1/3: development of a flat plate numerical model with experimental validation. Aerospace 7 (5), 62.

Villeneuve, E., Volat, C., Ghinet, S., 2020b. Numerical and experimental investigation of the design of a piezoelectric de-icing system for small rotorcraft part 2/3: investigation of transient vibration during frequency sweeps and optimal piezoelectric actuator excitation. Aerospace 7 (5), 49.

Villeneuve, E., Volat, C., Ghinet, S., 2020c. Numerical and experimental investigation of the design of a piezoelectric de-icing system for small rotorcraft part 3/3: numerical model and experimental validation of vibration-based de-icing of a flat plate structure. Aerospace 7 (5), 54.

Villeneuve, E., Blackburn, C., Volat, C., 2021a. Design and development of an experimental setup of electrically powered spinning rotor blades in icing wind tunnel and preliminary testing with surface coatings as hybrid protection solution. Aerospace 8, 98. https://doi.org/10.3390/aerospace8040098.

Villeneuve, E., Ghinet, S., Volat, C., 2021b. Experimental study of a piezoelectric de-icing system implemented to rotorcraft blades. Appl. Sci. 11, 9869. https://doi.org/10.3390/app11219869.

Zong, Z., 2022. A random pore model of sea ice for predicting its mechanical properties. Cold Reg. Sci. Technol. 195, 103473 https://doi.org/10.1016/j.coldregions.2021.103473.